AGU PUBLICATIONS

Geophysical Research Letters

RESEARCH LETTER
10.1002/2015GL064326

Key Points:
- Normal modes reveal radial anisotropy in the upper inner core
- Fast direction is radially outward, and slow direction is along the ICB
- Texture matches predictions from solidification processes or anisotropic growth

Supporting Information:
- Figures S1 and S2

Correspondence to:
K. H. Lythgoe,
khl43@cam.ac.uk

Citation:
Lythgoe, K. H., and A. Deuss (2015), The existence of radial anisotropy in Earth's upper inner core revealed from seismic normal mode observations, *Geophys. Res. Lett.*, *42*, 4841–4848, doi:10.1002/2015GL064326.

Received 22 APR 2015
Accepted 8 JUN 2015
Accepted article online 11 JUN 2015
Published online 29 JUN 2015

The existence of radial anisotropy in Earth's upper inner core revealed from seismic normal mode observations

Karen H. Lythgoe[1] and Arwen Deuss[2]

[1]Bullard Laboratories, University of Cambridge, Cambridge, England, [2]Department of Earth Sciences, Universiteit Utrecht, Utrecht, Netherlands

Abstract As we strive to understand the most remote region of our planet, one critical area of investigation is the uppermost inner core since its structure is related to solidification of outer core material at the inner core boundary (ICB). Previous seismic studies have used body waves to show that the top ~100 km of the inner core is isotropic. However, radial anisotropy cannot be uniquely determined by body wave observations. Alternatively, normal mode center frequencies are sensitive to spherically symmetric Earth structure, therefore may provide a constraint on the existence of radial anisotropy in the inner core. Here we show that normal mode center frequency measurements are compatible with 2–5% radial anisotropy in the top ~100 km of the inner core with a fast direction radially outward and a slow direction along the ICB. Given the uncertainties in the mineral physics and processes that produce anisotropy, the observed radial anisotropy may be reconciled with predictions based on either solidification processes or from texturing due to anisotropic growth.

1. Introduction

The seismic structure of the inner core boundary (ICB) is extremely important, since it is the site of inner core solidification. Solidification of outer core material provides energy in the form of latent heat and the release of light elements that drives the geodynamo, thus generating Earth's magnetic field. It has long been thought that the inner core boundary is a mushy layer, with solid iron crystallizing as dendrites perpendicular to the ICB [*Loper and Roberts*, 1981; *Fearne et al.*, 1981; *Shimizu et al.*, 2005; *Deguen et al.*, 2007]. This alignment could lead to radial anisotropy, i.e., transverse isotropy with a symmetry axis in the direction of Earth's radius. The existence of radial anisotropy in Earth's upper inner core thus provides key constraints on the type of processes occurring at the boundary between the solid inner core and the liquid outer core.

Seismology has revealed many intriguing structures within the inner core. Cylindrical anisotropy aligned with the Earth's rotation axis has been routinely observed by body waves [*Morelli et al.*, 1986] and is also seen in the anomalous splitting of core sensitive normal modes [*Woodhouse et al.*, 1986]. However, the uppermost ~100 km of the inner core is consistently imaged as seismically isotropic by body waves [*Song and Helmberger*, 1995; *Ouzounis and Creager*, 2001; *Waszek and Deuss*, 2011].

Since there is growing consensus that the inner core is composed of intrinsically anisotropic crystals, the most likely explanation for the seismic anisotropy is lattice-preferred orientation [*Stixrude and Cohen*, 1995; *Laio et al.*, 2000]. Crystals may become aligned due to solidification texturing, where crystal alignment is frozen in as the inner core solidifies [e.g., *Bergman*, 1997]. Alternatively, the anisotropy is produced later by deformation texturing or recrystallization, either due to preferential growth at the inner core boundary [*Yoshida et al.*, 1996], the Maxwell stress [*Karato*, 1999] or solid state inner core convection [*Jeanloz and Wenk*, 1988]. Some of these mechanisms lead to crystal alignment in the upper inner core.

Radial anisotropy is extensively studied in Earth's mantle but has not yet been investigated in Earth's inner core. Normal mode models of cylindrical anisotropy in the inner core find the strongest cylindrical anisotropy near the ICB [*Woodhouse et al.*, 1986; *Durek and Romanowicz*, 1999; *Ishii et al.*, 2002; *Beghein and Trampert*, 2003], although *Irving and Deuss* [2011] demonstrated that normal mode spectra are compatible with the presence of a shallow isotropic layer. Although an isotropic layer reconciles normal mode and body wave data, it is only one solution to the nonunique inverse problem. In particular, it is not incompatible with the presence of radial anisotropy, since radial anisotropy does not produce any variation of travel time with ray direction

that can be seen with body waves. Therefore, in order to observe radial anisotropy at the top of the inner core, normal mode center frequencies must be used.

2. Method

Earth's normal modes, or free oscillations, are long period (100–2000 s) standing waves along the surface and radius of the Earth and are seen as discrete peaks in the frequency domain. The frequency of oscillation is determined by the velocity and density structure inside the Earth. Spheroidal modes, denoted ${}_nS_l$, where n is the radial order or overtone number and l is the angular order, are used here, since they are sensitive to Earth's core. Modes with $l = 0$ are known as radial modes as they only exhibit radial motion, in which case n corresponds to the number of nodes of the standing wave along the radius of the Earth.

Due to symmetry constraints, normal modes have limited sensitivity to the center of the Earth. A number of modes have sensitivity to upper and intermediate regions of the inner core, and these modes are generally classified as either radial, PKIKP, or PKJKP modes [*Deuss*, 2008]. PKIKP modes are primarily sensitive to *P* wave velocity (V_p) in the inner core, where PKJKP modes are primarily sensitive to *S* wave velocity (V_s).

It has been shown that inner core spheroidal modes display distinct zonal degrees 2 and 4 splitting, which is attributed to cylindrical anisotropy in the bulk of the inner core, e.g., *Woodhouse et al.* [1986]. Splitting occurs when each mode multiplet is split into a set of $(2l+1)$ singlets with different frequencies. Zonal splitting function coefficients [i.e., C_{20} and C_{40} coefficients, *Woodhouse and Giardini*, 1985] describe cylindrical anisotropy, leaving mode center frequencies (the C_{00} coefficient) to describe spherically symmetric structure, such as radial anisotropy. Therefore, by measuring center frequency measurements in conjunction with splitting function coefficients [e.g., *Deuss et al.*, 2013], the effect of lateral heterogeneity (including inner core anisotropy) is accounted for in the splitting function, leaving the center frequencies to describe radial structure including radial anisotropy.

Here we investigate the presence of radial anisotropy in Earth's upper inner core using forward modeling of different inner core models. Normal mode catalogs are calculated for synthetic Earth models containing radial anisotropy in the inner core and are compared to real center frequency observations. The best fitting model is found by way of misfit analysis.

2.1. Radial Anisotropy

Radial and cylindrical anisotropies are both types of transverse isotropy with a vertical symmetry axis aligned along either Earth's radius or Earth's rotation axis, respectively. Radial anisotropy is introduced into the inner core by adapting the 1-D reference Earth model PREM (preliminary reference Earth model) [*Dziewonski and Anderson*, 1981] by introducing transverse isotropy in the inner core with a radial symmetry axis. In PREM, the Earth is isotropic, apart from the upper 220 km of the mantle where radial anisotropy is expressed in terms of the variation with depth of vertically and horizontally polarized *P* wave and *S* wave velocities—V_{pv}, V_{ph}, V_{sv} and V_{sh} respectively—and the velocity at intermediate wave directions, η. To investigate the effect of radial anisotropy only, the ratio of vertical to horizontal polarization is changed, without changing the isotropic velocity. This is done by expressing the anisotropic medium in terms of its equivalent isotropic medium, which corresponds to averaging over all incidence angles. For transverse isotropy (anisotropy with one symmetry axis), the Voigt bulk modulus is

$$\mathcal{K} = \frac{1}{9}(4A + C + 4F - 4N), \tag{1}$$

and the shear modulus is

$$\mu = \frac{1}{15}(A + C - 2F + 5N + 6L), \tag{2}$$

where A, C, F, L, and N are independent elastic parameters used to characterize an anisotropic medium with one symmetry axis, known as Love parameters. The Love parameters are equivalent to the following components of the elastic tensor

$$A = C_{11}; C = C_{33}; F = C_{13}; L = C_{44}; N = \frac{C_{11} - C_{12}}{2} = C_{66}. \tag{3}$$

For transverse isotropy with the symmetry axis in the radial direction, the Love parameters can also be expressed as

$$A = \rho V_{ph}^2, \tag{4}$$

$$C = \rho V_{pv}^2, \tag{5}$$

$$L = \rho V_{sv}^2, \tag{6}$$

$$N = \rho V_{sh}^2, \tag{7}$$

such that A and C are related to the compressional wave velocity perpendicular and parallel to the axis of symmetry, respectively, L and N are related to the shear wave velocity perpendicular and parallel to the axis of symmetry, respectively, and ρ is the density. The fifth parameter, F, is related to the speed of a wave traveling at intermediate angles to the symmetry axis. F is often expressed in terms of the nondimensional anisotropy parameter, η,

$$\eta = \frac{F}{(A - 2L)} \tag{8}$$

[*Anderson*, 1961]. The effective isotropic velocities are calculated

$$V_s = \sqrt{\frac{\mu}{\rho}}, \tag{9}$$

$$V_p = \sqrt{\frac{\mathcal{K} + \frac{4}{3}\mu}{\rho}}. \tag{10}$$

In order to test the effect of transverse anisotropy in the inner core on normal mode spectra, the values of η and the ratios V_{pv}/V_{ph} and V_{sv}/V_{sh} are changed without changing the Voigt bulk and shear modulus, therefore keeping the effective isotropic velocity the same as PREM. To do this, the anisotropy parameters ϕ and ξ are introduced from *Anderson* [1961], where

$$\phi = \frac{V_{pv}^2}{V_{ph}^2} = \frac{C}{A}, \tag{11}$$

$$\xi = \frac{V_{sh}^2}{V_{sv}^2} = \frac{N}{L}. \tag{12}$$

Equations (1), (2), (8), (11), and (12) are solved for the five Love parameters, A, C, N, L, and F, for given values of ϕ, ξ, η and using values of $\mathcal{K}$ and μ from PREM. Thus, new 1-D Earth models are created that contain an inner core with radial anisotropy, while having isotropic velocities that match PREM. Therefore, the effect of radial anisotropy on normal mode center frequencies can be isolated from changing the effective isotropic velocity.

2.2. Mode Catalogs

For each Earth model, new mode catalogs are computed using the method outlined in *Woodhouse* [1988]. Normal modes are computed by solving the wave equation exactly using an eigenfunction approach. Eigenfunctions and eigenfrequencies (normal mode frequencies) are computed using a numerical Runge-Kutta integrator. Since the mode catalog is calculated exactly, it automatically includes all nonlinear effects from 1-D variations [*Andrews et al.*, 2006; *Deuss*, 2008].

2.3. Data

The center frequencies predicted by the synthetic spectra are compared to previous measurements. Here the data set of *Deuss et al.* [2013] is used as it is the most recent and extensive, using a sizeable data set of large magnitude earthquakes. There are 19 PKIKP modes ($_8S_1$, $_{11}S_1$, $_{13}S_1$, $_{13}S_2$, $_{13}S_3$, $_{15}S_3$, $_{15}S_4$, $_{16}S_5$, $_{16}S_7$, $_{17}S_1$, $_{18}S_3$, $_{18}S_4$, $_{20}S_1$, $_{21}S_6$, $_{23}S_4$, $_{23}S_5$, $_{25}S_1$, $_{25}S_2$, $_{27}S_2$) and 14 PKJKP modes ($_3S_2$, $_6S_3$, $_8S_5$, $_9S_3$, $_9S_4$, $_{11}S_4$, $_{11}S_5$, $_{14}S_4$, $_{16}S_6$, $_{17}S_8$, $_{18}S_6$, $_{20}S_5$, $_{21}S_7$, $_{22}S_1$).

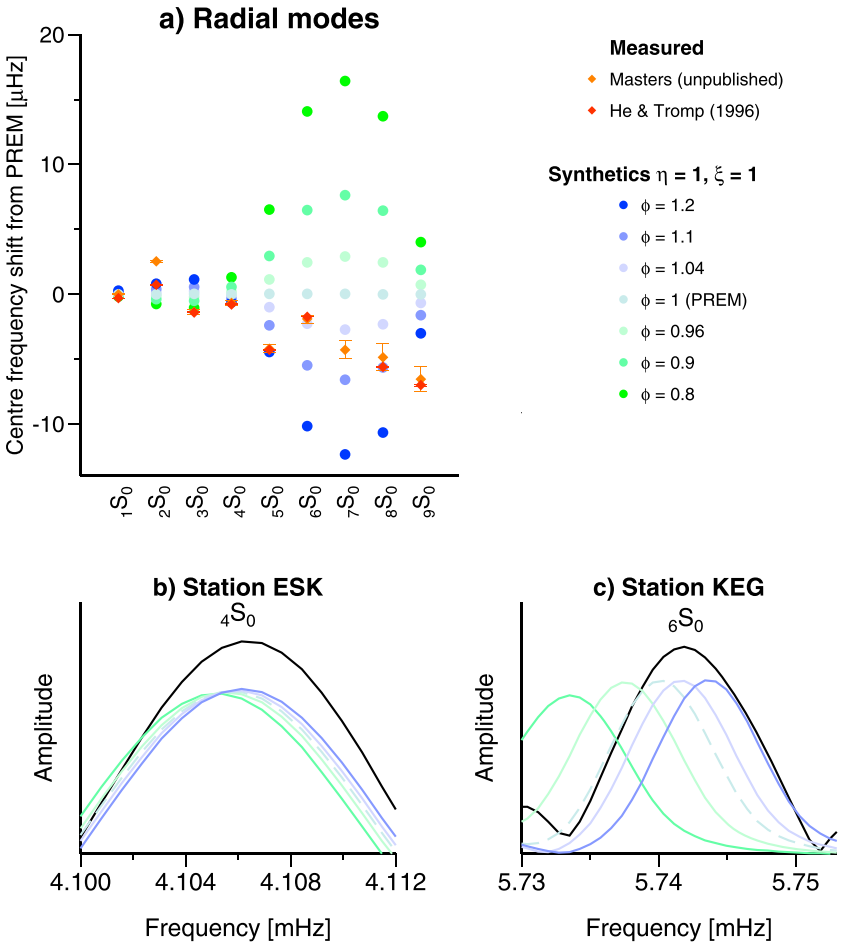

Figure 1. (a) Center frequency shifts from PREM for several synthetic radially anisotropic inner core models (green and blue dots), plus measured center frequency shifts (red dots) for *P* wave radial anisotropy in the upper 100 km of the inner core. Measured center frequencies are from *He and Tromp* [1996] and the Reference Earth Model web page (unpublished). (b) Spectra at station ESK (Eskdalemuir, Scotland) for the 1994 Bolivia earthquake (black), with predicted spectra for the synthetic Earth models above (PREM is shown as a dashed line). Data are Hann tapered between 20 and 70 h after the event. (c) Real and predicted spectra at station KEG (Egypt). Data are Hann tapered between 10 and 80 h after the event.

There are fewer studies looking at radial modes—*He and Tromp* [1996] provide the most recent published center frequency values; therefore, these have been used here. There are also several radial mode center frequency measurements available from the Reference Earth Model web page (http://igppweb.ucsd.edu/~gabi/rem.html). Although these measurements are not published, the center frequency for mode $_7S_0$ is used here, since it is not measured by *He and Tromp* [1996].

Data from 9 June 1994, $M_w = 8.2$, Bolivia earthquake are also used for comparison of real radial mode spectra with synthetic data. Synthetic seismograms for this event were calculated by summation of a complete catalog of normal modes [*Gilbert*, 1971] using the centroid moment tensor solution for the event [*Dziewonski et al.*, 1981]. Radial modes only depend on the 1-D structure and only consist of one singlet, thus splitting due to rotation, ellipticity, or heterogeneity (such as inner core anisotropy) does not occur and was not included in the synthetic seismograms.

2.4. Misfit

We define misfit as the difference between the observed (f_{data}) and synthetic ($f_{\text{synthetic}}$) center frequencies, summed over all modes,

$$\text{Misfit} = \sqrt{\frac{1}{N}\sum_{i=1}^{N}(f_{\text{data}} - f_{\text{synthetic}})_i^2}, \tag{13}$$

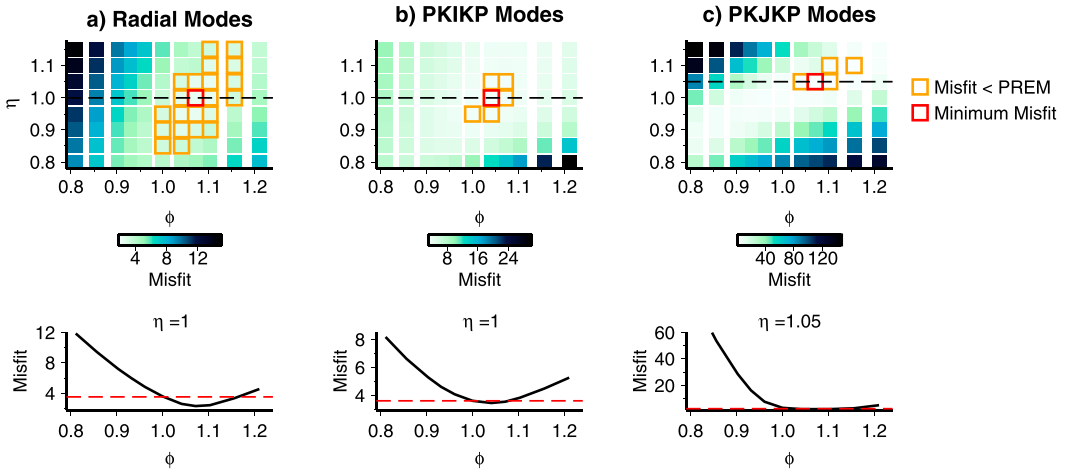

Figure 2. Misfits for models with varying ϕ and η values, assuming $\xi = 1$. Bottom row shows cross sections through the location of minimum misfit, with the red dashed line corresponding to the misfit for PREM. (a) Radial modes. (b) PKIKP modes. (c) PKJKP modes.

where N is the number of modes, such that the best fitting model to the data has the lowest misfit. Misfits are calculated for each Earth model, using all inner core sensitive modes measured in the studies of *He and Tromp* [1996] and *Deuss et al.* [2013]. Misfits are computed for center frequencies alone—not spectra—since center frequencies are only affected by spherically symmetric structure. Misfits are calculated separately for radial, PKIKP, and PKJKP modes.

3. Results

Results are firstly shown for synthetic Earth models with radial anisotropy in the upper 100 km of the inner core only, since this corresponds to the depth at which body waves find an isotropic layer. Earth models with radial anisotropy in the whole inner core are tested in section 3.4.

3.1. Radial Modes

We find that center frequencies of radial modes vary by several μHz in response to radial anisotropy. Figure 1a shows predicted center frequency shifts from PREM for an inner core with radial anisotropy in V_p, in the upper 100 km of the inner core only. The majority of radial mode center frequencies are best matched by models with V_{pv} greater than V_{ph}, i.e., $\phi > 1$. The effect of radial anisotropy can also be clearly seen in the frequency spectra of normal modes (Figures 1b and 1c). The spectra of the example modes, ${}_4S_0$ and ${}_6S_0$ shown, are again best matched by models with V_{pv} greater than V_{ph}.

We then perform a parameter search by systematically varying ϕ, ξ, and η values, in order to find the combination that best matches the center frequency data. There is almost no variation in misfit with ξ indicating that radial modes have very little sensitivity to shear anisotropy in the upper inner core. The resulting misfit plot for ϕ and η is shown in Figure 2a with models showing a misfit less than PREM highlighted. The best fitting models have $\phi \geq 1$ and η close to 1.

3.2. PKIKP and PKJKP Modes

The parameter search is also performed on PKIKP and PKJKP modes (Figures 2b and 2c). The best fitting models for PKIKP modes have η close to 1, with ϕ between 1 and 1.1, which is similar to the best fitting models for radial modes. Again, there is almost no variation in misfit with ξ.

The misfits for PKJKP modes are much higher than for other mode types. The frequency of certain PKJKP modes, such as ${}_8S_5$, ${}_9S_3$ and ${}_9S_4$, was reported by *Andrews et al.* [2006] to vary significantly with V_s, and it is found that mode ${}_{17}S_8$ is also strongly dependent on V_s. PKJKP modes have very large misfits for some models—for example, models with $\eta = 0.8$ or $\eta = 1.1$, and $\phi < 1$. Since PKJKP modes are sensitive to shear velocity, they should ideally provide the greatest constraints on ξ. However, although there is some variation

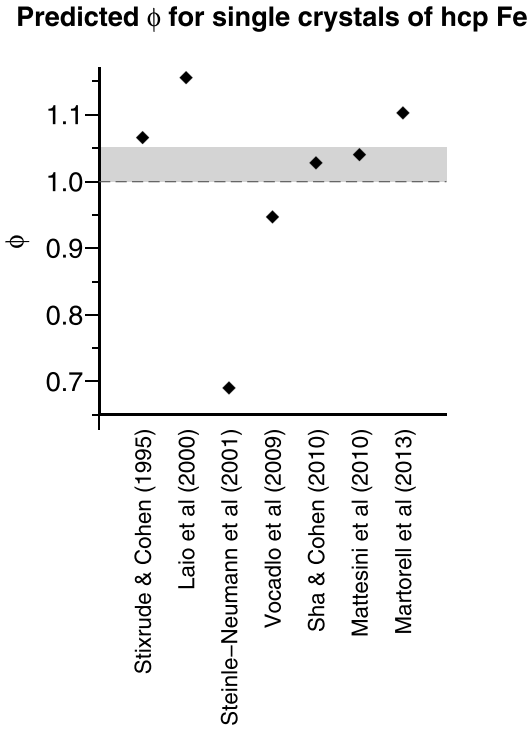

Figure 3. Predicted values of ϕ calculated from the elastic constants of several experimental and molecular dynamic studies. Assuming that the c axis is orientated radially, ϕ is calculated. Shaded region represents the range of ϕ implied by seismology.

in misfit with ξ, there is a trade-off with η and so ξ remains difficult to constrain (Figure S1 in the supporting information). The best fitting models for PKJKP modes have $\eta = 1$ or 1.1, with $\phi \geq 1$.

3.3. All Modes

For all mode types, the misfit is less than that for an isotropic inner core (PREM), when η is approximately 1 and when ϕ is > 1. The strongest dependency is on ϕ, with the best fitting models containing a layer with V_{pv} between 2 to 5% faster than V_{ph}. We find that $\eta = 0.8$ is a poor fit for all mode types, with $\eta = 1$ generally the best match.

3.4. Radial Anisotropy in the Whole Inner Core

Models with radial anisotropy throughout the whole inner core are also tested (see Figure S2). The only mode type to show any misfit reduction compared to PREM is radial modes, which are best fit by models with $\phi = 1$. It is clear for PKIKP and PKJKP modes that there is a trade-off between ϕ and ξ in the whole inner core. This suggests that normal modes are incompatible with the presence of constant radial anisotropy in the whole inner core.

4. Discussion and Conclusions

Normal mode center frequencies reveal that the top of the inner core may be radially anisotropic, with a fast compressional direction along Earth's radius. This has been shown through forward modeling of synthetic Earth models with radial anisotropy added to the top 100 km of the inner core. The forward modeling indicates that in the uppermost inner core ϕ is greater than 1 and η is approximately 1. Normal mode center frequencies have little sensitivity to ξ and so constraints on the shear radial anisotropy structure of the inner core remain elusive.

A 100 km thick layer was chosen to match the thickness of the isotropic layer imaged by body waves. Although the depth extent of radial anisotropy has not been tested, it is clear from section 3.4 that normal mode observations are incompatible with constant radial anisotropy throughout the whole inner core. In the future, a full 3-D inversion for the whole Earth—using mantle and inner core sensitive modes—is needed to better analyze the properties and depth extent of the radially anisotropic layer. Simultaneously inverting for the mantle is required to account for any trade-offs with radial structure there.

The proposed radial anisotropy model, with a faster radial direction in the top of the inner core, will also have an effect on compressional body waves. PKIKP waves which travel parallel to the ICB in the uppermost inner core will be delayed; PKIKP waves which travel deeper in the inner core and more perpendicular to the ICB will arrive faster. This effect may (incorrectly) be interpreted as isotropic velocity variations with depth, i.e., a slow velocity in the top and faster velocity in the deeper inner core. Thus, body wave observations need to be corrected for the existence of radial anisotropy.

Assuming the c axis is radially aligned, ϕ is calculated from estimated elastic constants, shown in Figure 3. The majority of studies [*Stixrude and Cohen*, 1995; *Sha and Cohen*, 2010; *Mattesini et al.*, 2010; *Laio et al.*, 2000; *Martorell et al.*, 2013] predict the c axis to be the fast crystal direction and so ϕ is greater than 1 (Figure 3). This implies that the seismically observed value of $\phi \sim 1.02–1.05$ can be explained by complete or partial

alignment of crystals in the upper inner core, with the *c* axis orientated along Earth's radius. Alternatively, studies by *Steinle-Neumann et al.* [2001] and *Vocadlo et al.* [2009] predict the *c* axis to be the slowest direction. However, due to the agreement between experimental and theoretical studies [*Tateno et al.*, 2010], and since the theoretical approximations used by *Steinle-Neumann et al.* [2001] have been questioned [*Gannarelli et al.*, 2005], we assume a fast *c* axis in the remaining discussion.

Texture at the top of the inner core results from either solidification texturing or later recrystallization due to internal deformation. Dendrites are predicted to grow along the direction of maximum heat flux which is locally radial at the ICB, thereby aligning the *c* axis of hcp crystals along the plane of the ICB [*Bergman*, 1997]. Assuming the *c* axis is the fast crystallographic direction [*Stixrude and Cohen*, 1995; *Sha and Cohen*, 2010; *Martorell et al.*, 2013], this results in anisotropy of the opposite orientation to that observed seismically. However, it is possible that convective flow within a mushy zone aligns *c* axes along Earth's radius [*Bergman et al.*, 2002, 2003], although more work needs to be done to verify these experiments. It is likely that the presence of fluid will significantly affect the seismic signature, and so radial anisotropy could be an indicator of a thick mushy layer at the inner core boundary. Lastly, it remains possible that the *c* axis is actually the slow direction of hcp crystals, as has been suggested by several authors [*Steinle-Neumann et al.*, 2001; *Vocadlo et al.*, 2009].

One promising explanation for the seismically observed radial anisotropy is anisotropic inner core growth [*Yoshida et al.*, 1996]. Faster growth of the inner core in equatorial regions compared to polar regions produces an internal flow which causes stress induced recrystallization. The flow pattern depends on several uncertain parameters, such as the inner core's viscosity, stratification, and the amount of fluid it contains. However, it is possible to generate a texture with the fast direction of hcp crystals aligned along Earth's radius in the upper inner core and along Earth's rotation axis in the deeper inner core [*Yoshida et al.*, 1996; *Deguen and Cardin*, 2011; *Lincot et al.*, 2014]. Therefore, by matching the seismic observations to predicted textures, there is potential to better constrain elusive properties of the inner core, such as its viscosity.

Acknowledgments
We would like to thank Ralph de Wit, Jeannot Trampert, Jerome Neufeld, and John Rudge for helpful discussions. This work has been partly funded through the European Research Council under the European Community's Seventh Framework Programme (FP7/2007-2013)/ERC grant agreement number 204995. A.D. was also funded by a Philip Leverhulme Prize.

The Editor thanks Michael I. Bergman and an anonymous reviewer for their assistance evaluating this paper.

References

Anderson, D. L. (1961), Elastic wave propagation in layered anisotropic media, *J. Geophys. Res.*, *66*, 2953–2963.
Andrews, J., A. Deuss, and J. Woodhouse (2006), Coupled normal-mode sensitivity to inner core shear velocity and attenuation, *Geophys. J. Int.*, *167*, 204–212.
Beghein, C., and J. Trampert (2003), Robust normal mode constraints on inner core anisotropy from model space search, *Science*, *299*, 552–555.
Bergman, M. I. (1997), Measurements of elastic anisotropy due to solidification texturing and the implications for the Earth's inner core, *Nature*, *389*, 60–63.
Bergman, M. I., D. Cole, and J. Jones (2002), Preferred crystal orientations due to melt convection during directional solidification, *J. Geophys. Res.*, *107*, ECV 6–1–6-8, doi:10.1029/2001JB000601.
Bergman, M. I., S. Agrawal, and M. S. Carter (2003), Transverse solidification textures in hexagonal close-packed alloys, *J. Crystal Growth*, *255*, 204–211.
Deguen, R., and P. Cardin (2011), Thermochemical convection in Earth's inner core, *J. Geophys. Res.*, *187*, 1101–1118, doi:10.1111/j.1365-246X.2011.05222.x.
Deguen, R., T. Alboussière, and D. Brito (2007), On the presence and structure of a mush at the inner core boundary of the Earth, *Phys. Earth Planet. Inter.*, *274*, 1887–1891.
Deuss, A. (2008), Normal mode constraints on shear and compressional wave velocity of the Earth's inner core, *Earth Planet. Sci. Lett.*, *268*, 364–375.
Deuss, A., J. Ritsema, and H. van Heijst (2013), A new catalogue of normal mode splitting function measurements up to 10 mHz, *Geophys. J. Int.*, *193*, 920–937.
Durek, J. J., and B. Romanowicz (1999), Inner core anisotropy inferred by direct inversion of normal mode spectra, *Geophys. J. Int.*, *139*, 599–622.
Dziewonski, A. M., and D. L. Anderson (1981), Preliminary reference Earth model, *Phys. Earth Planet. Inter.*, *25*, 297–356.
Dziewonski, A. M., T. A. Chou, and J. H. Woodhouse (1981), Determination of earthquake source parameters from waveform data for studies of global and regional seismicity, *J. Geophys. Res.*, 2825–2852.
Fearne, D. R., D. E. Loper, and P. H. Roberts (1981), Structure of the Earth's inner core, *Nature*, *292*, 232–233.
Gannarelli, C. M. S., D. Alfe, and M. J. Gillan (2005), The axial ratio of hcp iron at the conditions of the Earth's inner core, *Phys. Earth Planet. Inter.*, *152*, 67–77.
Gilbert, F. (1971), Excitation of normal modes of the Earth by earthquake sources, *Geophys. J. R. Astron. Soc.*, *22*, 223–226.
He, X., and J. Tromp (1996), Normal mode constraints on the structure of the mantle and core, *J. Geophys. Res.*, *101*, 20, 053–20,082.
Irving, J. C. E., and A. Deuss (2011), Stratified anisotropic structure at the top of Earth's inner core: A normal mode study, *Phys. Earth Planet. Inter.*, *186*, 59–69.
Ishii, M., J. Tromp, A. M. Dziewonski, and G. Ekstrom (2002), Joint inversion of normal mode and body wave data for inner core anisotropy 1. Laterally homogenous anisotropy, *J. Geophys. Res.*, *107*, 2379, doi:10.1029/2001JB000712.
Jeanloz, R., and H. R. Wenk (1988), Convection and anisotropy of the inner core, *Geophys. Res. Lett.*, *15*, 72–75.
Karato, S. (1999), Seismic anisotropy of the Earth's inner core resulting from flow induced by Maxwell stresses, *Nature*, *402*, 871–873.
Laio, A., S. Bernard, G. L. Chiarottie, S. Scandolo, and E. Tosatti (2000), Physics of iron at Earth's core conditions, *Science*, *287*, 1027–1030.
Lincot, A., R. Deguen, S. Merkel, and P. Cardin (2014), Seismic response and anisotropy of a model hcp iron inner core, *C. R. Geosci.*, *346*, 148–157.

Loper, D. E., and P. H. Roberts (1981), A study of conditions at the inner core boundary of the Earth, *Phys. Earth Planet. Inter.*, *24*, 302–307.
Martorell, B., J. Brodholt, I. G. Wood, and L. Vocadlo (2013), The effect of nickel on properties of iron at the conditions of Earth's inner core: Ab initio calculations of seismic wave velocities of Fe-Ni alloys, *Earth Planet. Sci. Lett.*, *365*, 143–151.
Mattesini, M., A. Belonoshko, E. Buforn, M. Ramirez, S. Simak, A. Udias, H. Mao, and R. Ahuja (2010), Hemispherical anisotropic patterns of the Earth's inner core, *Proc. Natl. Acad. Sci. U.S.A.*, *107*, 9507–9512.
Morelli, A., A. M. Dziewonski, and J. H. Woodhouse (1986), Anisotropy of the inner core inferred from PKIKP travel times, *Geophys. Res. Lett.*, *13*, 1545–1548.
Ouzounis, A., and K. C. Creager (2001), Isotropy overlying anisotropy at the top of the inner core, *Geophys. Res. Lett.*, *28*, 4331–4334.
Sha, X., and R. E. Cohen (2010), First-principles thermal equation of state and thermoelasticity of hcp Fe at high pressures, *Phys. Rev.*, *81*, 94,105, doi:10.1103/PhysRevB.81.094105.
Shimizu, H., J. P. Poirier, and J. L. LeMouel (2005), On crystallization at the inner core boundary, *Phys. Earth Planet. Inter.*, *151*, 37–51.
Song, X. D., and D. V. Helmberger (1995), Depth dependence of anisotropy of Earth's inner core, *J. Geophys. Res.*, *100*, 9805–9816.
Steinle-Neumann, G., L. Stixrude, R. E. Cohen, and O. Gulseren (2001), Elasticity of iron at the temperature of the Earth's inner core, *Nature*, *413*, 57–60.
Stixrude, L., and R. E. Cohen (1995), High-pressure elasticity of iron and anisotropy of the Earth's inner core, *Science*, *267*, 1972–1975.
Tateno, S., K. Hirose, Y. Ohishi, and Y. Tatsumi (2010), The structure of iron in the Earth's inner core, *Science*, *330*, 359–361.
Vocadlo, L., D. Dobson, and I. Wood (2009), Ab initio calculations of the elasticity of hcp-Fe as a function of temperature at inner-core pressure, *Earth Planet. Sci. Lett.*, *288*, 534–538.
Waszek, L., and A. Deuss (2011), Distinct layering in the hemispherical seismic velocity structure of Earth's upper inner core, *J. Geophys. Res.*, *116*, B12313, doi:10.1029/2011JB008650.
Woodhouse, J. H. (1988), The calculation of the eigenfrequencies and eigenfunctions of the free oscillations of the Earth and the Sun, in *Seismological Algorithms*, edited by D. J. Doornbos, pp. 321–370, Acad. Press, San Diego, Calif.
Woodhouse, J. H., and D. Giardini (1985), Inversion for the splitting function of isolated low order normal mode multiplets, *Eos Trans. AGU*, *66*, 300.
Woodhouse, J. H., D. Giardini, and X. D. Li (1986), Evidence for inner core anisotropy from free oscillations, *Geophys. Res. Lett.*, *13*, 1549–1552.
Yoshida, S., I. Sumita, and M. Kumazawa (1996), Growth model of the inner core coupled with outer core dynamics and the resulting elastic anisotropy, *J. Geophys. Res.*, *101*, 28,085–28,103.